Journal of Materials Chemistry B

ROYAL SOCIETY OF CHEMISTRY

PAPER

View Article Online
View Journal

Cite this: DOI: 10.1039/d6tb00517a

A shikonin-based self-assembled nanomedicine alleviates DSS-induced colitis involving HDC-associated histamine regulation and gut microbiota modulation

Wang Zhang,[a] Jingrou Sun,[a] Ying Ou,[a] Jing Zhang,[a] Yilan Bai,[a] Jingxi Hong,[a] Lingchang Meng,[b] Yi Song,[b] Tiepeng Wang,[b] Zhiting Sun*[b] and Jing Wu*[ab]

Ulcerative colitis (UC) is a chronic inflammatory disorder of the intestine characterized by recurrent episodes. Current therapies exhibit limited efficacy and raise safety concerns. This study aimed to enhance the water solubility of the natural compound shikonin and improve its therapeutic efficacy by developing novel metal-phenolic nanoparticles. Zn-shikonin-PEG hybrid nanoparticles (Zn-SHK-PEG NPs) were synthesized by coordinating Zn^{2+} with shikonin and functionalizing the complex with polyethylene glycol (PEG). Dextran sulfate sodium (DSS)-induced colitis was employed to evaluate the therapeutic potential and mechanisms of the nanoparticles. Treatment with Zn-SHK-PEG NPs markedly alleviated weight loss and colon shortening, decreased the disease activity index (DAI), and reduced histopathological injury. Mechanistic investigations suggested that the nanoparticles reduced histidine decarboxylase (HDC) expression, which was associated with PKM2 regulation, accompanied by decreased histamine (HA) levels and suppressed inflammation. Furthermore, Zn-SHK-PEG NPs altered the gut microbiota composition, including enrichment of *Akkermansia muciniphila*, which may also contribute to the overall therapeutic effect. In summary, Zn-SHK-PEG NPs ameliorated DSS-induced colitis, and the therapeutic effects were associated with the regulation of the HDC/histamine axis, suppression of inflammatory responses, and modulation of gut microbiota. These findings suggest that Zn-SHK-PEG NPs may represent a potential strategy for ulcerative colitis treatment.

Received 6th March 2026,
Accepted 7th May 2026

DOI: 10.1039/d6tb00517a

rsc.li/materials-b

1. Introduction

Ulcerative colitis (UC) is a chronic and recurrent inflammatory disease, mainly involving the mucosal layers of the colon.[1] This condition is influenced by impairment of the epithelial barrier and immune dysregulation.[2] As of 2023, approximately 5 million individuals worldwide are affected by ulcerative colitis, with the cumulative incidence in Western countries continuing to rise.[3,4] 5-Aminosalicylic acid (5-ASA) is currently recommended as treatment for mild to moderate UC. For patients with severe UC, therapeutic strategies typically involve corticosteroids, immunosuppressants, and biologics commonly applied in clinical settings.[5] Additionally, novel small molecule drugs have demonstrated significant efficacy.[6,7] Targeted therapies directed at tumor necrosis factor-like ligand 1A have exhibited therapeutic potential.[8] However, the aforementioned treatments present certain limitations in clinical application. For instance, 5-ASA is sometimes ineffective, while prolonged corticosteroid use may result in adverse effects, including adrenal suppression, immunosuppression, Cushing-like symptoms, and osteoporosis.[9] Immunosuppressants, such as azathioprine and methotrexate, carry an increased risk of hepatotoxicity.[10] Hence, the development of therapeutic strategies with enhanced precision, improved safety, and better cost-effectiveness is urgently required.

Shikonin (SHK) is a natural naphthoquinone isolated from *Lithospermum erythrorhizon* and has been reported to exhibit anti-inflammatory, antioxidant, and antitumor effects in multiple studies. SHK can alleviate isoproterenol-induced acute myocardial infarction by inhibiting Pyruvate Kinase M2 (PKM2).[11] It can also mitigate osteoarthritis and rheumatoid arthritis by suppressing the MAPK signaling pathway.[12,13] Moreover, SHK can regulate the gut microbiota to relieve acute inflammation.[14] The biomedical application of SHK is, however, constrained by several of its intrinsic properties, notably

[a] *Department of Traditional Chinese Medicine, Nanjing Drum Tower Hospital, Nanjing Drum Tower Hospital Clinical College of Nanjing University of Chinese Medicine, Nanjing 210008, People's Republic of China. E-mail: wujing@njucm.edu.cn*

[b] *The Institute of Chinese Medicine of Nanjing University, Nanjing Drum Tower Hospital, Affiliated Hospital of Medical School, Nanjing University, Nanjing 210008, People's Republic of China. E-mail: szt19910817@163.com*

inadequate solubility and low bioavailability.[15] To circumvent these pharmacokinetic limitations, metal-phenolic networks (MPNs) have emerged as a promising platform for drug delivery.[16] By leveraging the robust coordination between bioactive metal ions and phenolic ligands, MPNs facilitate the construction of carrier-free nanostructures that maximize drug loading while ensuring excellent biocompatibility.[17–19] Moreover, MPNs can integrate multiple functions, such as drug delivery, antioxidant activity, anti-inflammation, and gut microbiota regulation, thus achieving various synergistic therapeutic effects.[20–23] Despite the structural advantages of MPNs, the harsh and dynamic physiological environment within the gastrointestinal tract poses a significant challenge to the stability and targeted delivery to conventional coordination complexes. To address these challenges, we strategically integrated surface engineering using polyethylene glycol (PEG) to enhance the gastrointestinal performance of the Zn-SHK framework. PEGylation provides critical steric stabilization that shields the pH-sensitive coordination bonds from premature dissociation in the stomach, while simultaneously endowing the nanoparticles with mucus-penetrating ''stealth'' characteristics to ensure deep penetration into the inflamed colonic tissue.[23]

This study aimed to synthesize Zn-SHK-PEG nanoparticles (Zn-SHK-PEG NPs) and evaluate their effects in DSS-induced colitis. The results showed that Zn-SHK-PEG NPs alleviated DSS-induced colitis and were associated with reduced HDC expression, lower serum histamine levels, suppressed inflammatory cell infiltration, improved intestinal barrier integrity, and altered gut microbiota composition. These findings suggest that combining metal-assisted self-assembly with natural products may provide a potential formulation strategy for ulcerative colitis and related inflammatory disorders.

2. Materials and methods

2.1. Materials

Zinc chloride was obtained from Aladdin (Shanghai, China), and Shikonin was purchased from MedChemExpress (Shanghai, China). Polyethylene glycol was purchased from Aladdin (Shanghai, China). Dextran sulfate sodium salt was purchased from MP Biomedicals (Santa Ana, CA, USA). 5-Aminosalicylic acid was purchased from Sigma-Aldrich (St. Louis, MO, USA). Lipopolysaccharide was purchased from Sigma-Aldrich (St. Louis, MO, USA). ELISA kits for interleukin-1β, interleukin-6, and histamine were purchased from Jianglai Biotechnology (Shanghai, China). Histamine was purchased from Sigma-Aldrich (St. Louis, MO, USA).

2.2. Synthesis of Zn-SHK-PEG NPs

1 mL of shikonin was prepared in ethanol at 4 mg mL^{-1}. With the molar ratio of $ZnCl_2$ to SHK set at 3 : 1, the SHK ethanol solution was added dropwise into 10 mL of $ZnCl_2$ aqueous solution while stirring. Continuous stirring at room temperature for 1 h formed Zn-SHK nanoparticles. The dispersion was centrifuged at 12 000 rpm for 20 min, then a polyethylene glycol (25 mg mL^{-1}) ethanol solution was added and the mixture was stirred overnight at room temperature. The ethanol was removed by rotary evaporation and the product was redissolved in pure water or 1× PBS for subsequent experiments.

2.3. Characterization of Zn-SHK-PEG NPs

The morphology of the Zn-SHK-PEG NPs was observed using transmission electron microscopy (TEM, Tecnai G2 F20, FEI, USA). The hydrodynamic diameter, polydispersity index (PDI), and zeta potential were measured using a Zetasizer Lab analyzer (Malvern Panalytical, UK). The time-dependent hydrodynamic diameter of the Zn-SHK-PEG NPs was further monitored in different media, including ultrapure water, PBS, 10% FBS, simulated gastric fluid, and simulated intestinal fluid, to evaluate their stability. UV-Vis absorption spectra were recorded using a UV-Vis spectrophotometer (UV-2700i, Shimadzu, Japan). Fourier transform infrared spectroscopy (FTIR) was carried out using a Nicolet iS10 spectrometer (ThermoFisher, USA). X-ray photoelectron spectroscopy (XPS) was performed using an ESCALAB 250Xi spectrometer (ThermoFisher, USA) to analyze the elemental composition and chemical states of Zn-SHK-PEG NPs. The zinc content of the Zn-SHK-PEG NPs was measured using inductively coupled plasma optical emission spectroscopy (ICP-OES, Thermo ICPOES 7200, ThermoFisher, USA). The cumulative release of SHK from different nanoparticles was studied by the dialysis method to investigate the release behavior of different nanoparticles in different media.

2.4. Cytotoxicity detection

The cytotoxicity of SHK, Zn-SHK NPs, and Zn-SHK-PEG NPs was evaluated in RAW264.7 and Caco-2 cells using a CCK-8 assay. The cells were seeded uniformly into a 96-well plate at 1×10^4 cells per well. Drugs at varying concentrations were then applied for 24 h. Subsequently, 10 μL of CCK-8 solution were added to each well before the end of treatment, and the plates were incubated in the dark for 30 min, and the absorbance was measured at 450 nm.

2.5. Establishment and treatment of dextran sulfate sodium-induced colitis

Male C57BL/6 mice (6-8 weeks old) were supplied by SPF Biotechnology Co., Ltd, (Beijing, China). The mice were randomly assigned to the control group (CON), DSS group, 5-aminosalicylic acid group (5-ASA) (150 mg kg^{-1}), $ZnCl_2$ group (5.67 mg kg^{-1}), SHK group (12 mg kg^{-1}) and Zn-SHK-PEG NPs group (at an equivalent shikonin dose of 12 mg kg^{-1}) (n = 6). 5-ASA, $ZnCl_2$ and SHK were dissolved in 0.05% sodium carboxymethyl cellulose solution. And Zn-SHK-PEG NPs were dissolved in ultrapure water. The CON and DSS groups received the corresponding vehicles. All treatments were administered by oral gavage. Except for the control group, the mice received 2.5% (w/v) DSS in drinking water for 7 days, followed by sterile water for 3 days. All animal experiments were approved by the Experimental Animal Ethics Committee of Nanjing Hospital Affiliated to Nanjing Medical University (Approval No. DWSY-24155613) and were conducted in accordance with institutional guidelines.

2.6. Assessment of colitis

Body weight, fecal consistency, and fecal blood were recorded each day to calculate the Disease Activity Index (DAI) score (Table S1). Mice were euthanized with isoflurane and colons were collected, and their length was measured. Colonic contents were aseptically collected, immediately snap-frozen in liquid nitrogen, and stored at −80 °C until further analysis. Distal colon segments were fixed in 4% paraformaldehyde for hematoxylin and eosin (H&E).

2.7. Enzyme-linked immunosorbent assay (ELISA)

Serum levels of the inflammatory cytokines IL-1β and IL-6 were quantified using commercially available ELISA kits, following the manufacturers' protocols.

2.8. Immunohistochemistry

Paraffin-embedded colonic sections were deparaffinized, subjected to antigen retrieval in citrate buffer (pH 6.0), and blocked with 5% BSA. Sections were incubated overnight at 4 °C with primary antibodies against ZO-1 and Occludin (Proteintech, Wuhan, China), followed by HRP-conjugated secondary antibodies, DAB visualization, hematoxylin counterstaining, and light microscopy.

2.9. Immunofluorescence

Paraffin-embedded colonic sections were deparaffinized, subjected to antigen retrieval, and blocked before overnight incubation at 4 °C with primary antibodies against F4/80 (ABclonal, Wuhan, China), HDC (PAG476Hu01, Cloud-Clone Corp, Wuhan, China), tryptase (ABclonal, Wuhan, China), and CD117 (Abmart, Shanghai, China). Sections were then incubated with fluorescent secondary antibodies, counterstained with DAPI, and imaged by fluorescence microscopy.

2.10. Reverse transcription quantitative PCR

Total RNA was extracted using Trizol reagent and then reverse-transcribed to cDNA. β-actin served as the internal control; primer sequences are listed in Table S2.

2.11. Western blotting analysis

Total protein was resolved by 10% SDS-PAGE, followed by transfer onto PVDF membranes. The membranes were incubated with primary antibodies against histidine decarboxylase (Abcam, Cambridge, UK) and cyclooxygenase-2 (ABclonal, Wuhan, China). After incubation with HRP-conjugated secondary antibodies, protein signals were visualized using enhanced chemiluminescence (ECL). The band intensities were quantified with ImageJ software.

2.12. *In vitro* treatment of RAW264.7 macrophages

RAW264.7 cells were cultured in DMEM supplemented with 10% fetal bovine serum and 1% penicillin streptomycin at 37 °C in a humidified incubator containing 5% CO_2. For the *in vitro* experiments, cells were pretreated with free SHK or Zn-SHK-PEG NPs at the same equivalent SHK concentration of 0.5 μg mL^{-1} for 2 h, followed by stimulation with LPS (100 ng mL^{-1}) for 24 h.

2.13. Small interfering RNA transfection

Small interfering RNAs targeting HDC (si-HDC) and PKM2 (si-PKM2), together with a non-targeting control siRNA (si-Control), were designed and synthesized by GenePharma (Shanghai, China). The cells were transfected when confluence reached approximately 30%–50%. According to the reagent instructions, siRNAs were delivered using CALNP RNAi *in vitro* transfection reagent. Cells were collected 24 h after transfection, total RNA was extracted, and HDC and PKM2 mRNA levels were measured by RT-qPCR to assess silencing efficiency. The experimental conditions comprised four groups: blank control (CON), LPS stimulation, LPS + siRNA and LPS + siRNA + Zn-SHK-PEG NPs. Transfections for each siRNA group were performed as described above. Cells were harvested after LPS (100 ng mL^{-1}) stimulation for 24 h.

2.14. Metagenomic sequencing analysis

Fecal samples from the CON, DSS, and Zn-SHK-PEG NPs groups underwent metagenomic sequencing. Genomic DNA was extracted, quality checked, and fragmented to 350 bp using a Covaris M220, followed by paired-end (PE) library construction and sequencing on the Illumina NovaSeq platform. After quality control and host genome removal, *de novo* assembly was performed with MEGAHIT (v1.1.2). Genes were predicted using Prodigal, and a non-redundant gene catalog was generated. Taxonomic and functional annotation was conducted by aligning gene sequences to the NR and KEGG databases using DIAMOND. Diversity and intergroup difference analyses were carried out based on the annotation results. All bioinformatic analyses were performed on the Majorbio Cloud Platform.

2.15. Statistical analysis

Data are presented as mean ± SD or SEM. Statistical analyses were performed using SPSS 25.0. Student's *t*-test was used for two-group comparisons, and one-way ANOVA with Tukey's *post hoc* test for multiple comparisons. When normality was not met, the Kruskal–Wallis test followed by Wilcoxon rank-sum test with FDR correction was applied. A p value < 0.05 was considered statistically significant ($^{*}p < 0.05$, $^{**}p < 0.01$, $^{***}p < 0.001$).

3. Results and discussion

3.1. The fabrication and characterization of Zn-SHK-PEG NPs

The phenolic hydroxyl groups of SHK rapidly self-assembled with zinc ions, resulting in the preparation of Zn-SHK nanoparticles (Fig. 1A). TEM revealed that individual particles showed approximately spherical or irregularly spherical morphologies (Fig. 1B). The ultraviolet absorption spectrum demonstrated that the characteristic absorption peak of Zn-SHK-PEG NPs closely resembled that of SHK, indicating successful coordination of $ZnCl_2$ with SHK (Fig. 1C). Dynamic light scattering (DLS) results showed that the Zn-SHK-PEG NPs had

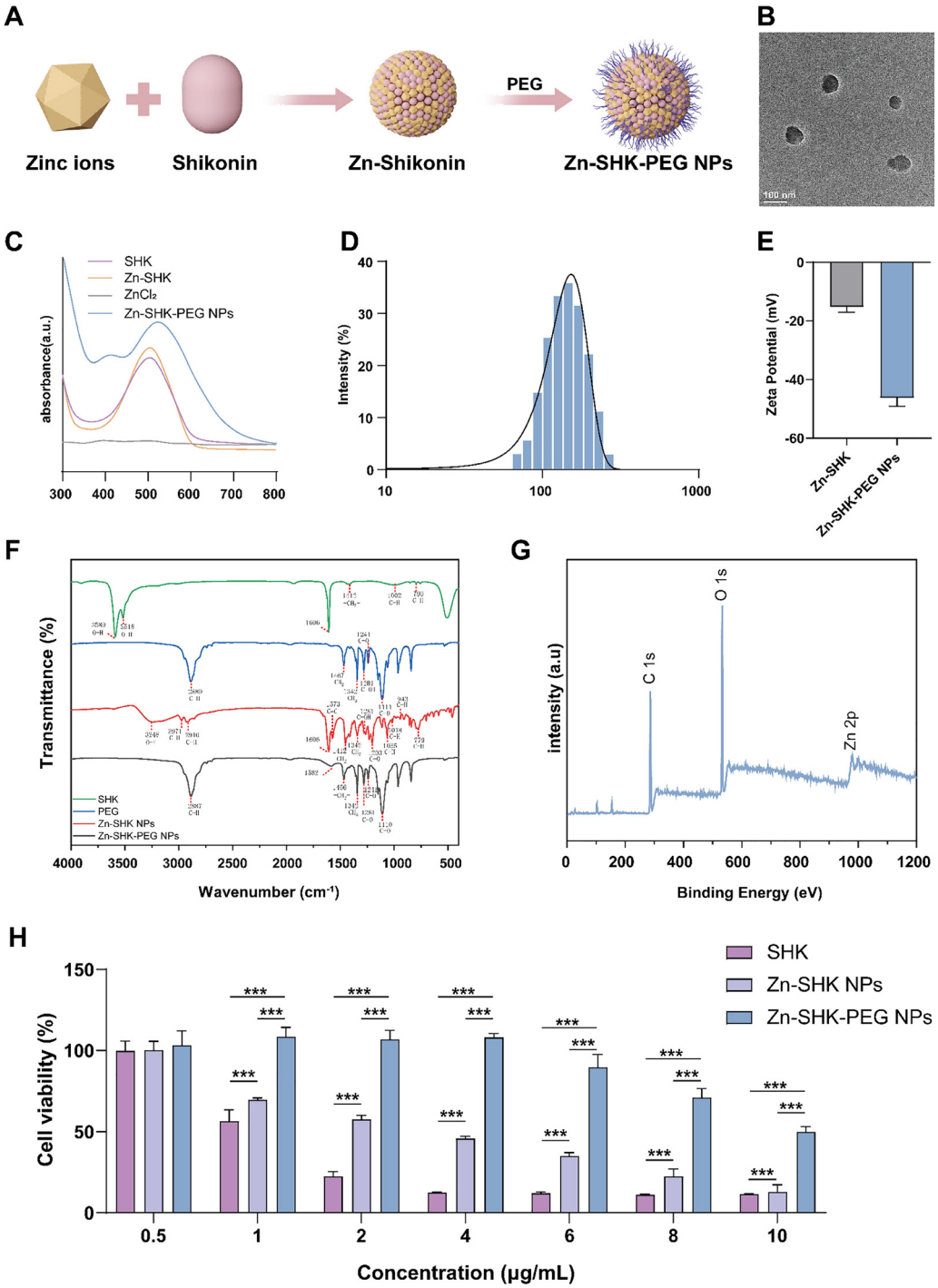

Fig. 1 The synthesis and characterization of Zn-SHK-PEG NPs. (A) Schematic diagram of Zn-SHK-PEG NPs synthesis. (B) Representative transmission electron microscopy (TEM) image of Zn-SHK-PEG NPs. (C) UV-Vis absorption spectrum of Zn-SHK-PEG NPs. (D and E) Particle size and zeta potential of Zn-SHK-PEG NPs. (F) FTIR spectra of SHK, PEG, Zn-SHK NPs, and Zn-SHK-PEG NPs. (G) X-ray photoelectron spectroscopy (XPS) survey spectrum of Zn-SHK-PEG NPs. (H) Cytotoxicity assays of SHK, Zn-SHK NPs and Zn-SHK-PEG NPs at different concentrations (at equivalent shikonin concentration) on RAW264.7 cells, n = 3.

an average hydrodynamic diameter of 148.43 ± 12.76 nm with a PDI of 0.29 (Fig. 1D). The zeta potentials of the Zn-SHK NPs and Zn-SHK-PEG NPs were −15.23 ± 1.83 mV and −46.215 ± 2.91 mV, respectively (Fig. 1E). The formation of Zn-SHK-PEG NPs was further confirmed by FTIR analysis. As shown in Fig. 1F, free SHK exhibited characteristic O–H stretching vibrations at 3589 and 3518 cm^{-1}, as well as an aromatic skeleton vibration at 1606 cm^{-1}. After coordination with Zn^{2+}, the O–H absorption band shifted to 3248 cm^{-1} in the Zn-SHK NPs, accompanied by the weakened C–OH stretching vibration at 1281 cm^{-1},

indicating the coordination interaction between Zn^{2+} and the oxygen-containing groups of SHK. In the spectrum of the Zn-SHK-PEG NPs, the characteristic absorption bands at 2887, 1466, 1342, and 1281–1110 cm^{-1} were assigned to C–H stretching, $–CH_2–$ bending, $–CH_3$ bending, and C–O stretching vibrations, respectively, demonstrating the successful incorporation of PEG into the Zn-SHK nanoparticle system. XPS analysis further confirmed the presence of C, O, and Zn elements in Zn-SHK-PEG NPs (Fig. 1G). The high-resolution Zn 2p spectrum showed characteristic Zn $2p_{3/2}$ and Zn $2p_{1/2}$ peaks, while the C 1s and O 1s spectra revealed C–C, C–O, and C═O components (Fig. S1). Together, these FTIR and XPS results support the formation of Zn^{2+}-assisted SHK-based self-assembled nanoparticles rather than a simple physical mixture. The encapsulation efficiency of SHK within Zn-SHK-PEG NPs was determined based on the amount of free SHK remaining in the supernatant following centrifugation. Utilizing a UV-Vis calibration curve at 516 nm, the encapsulation efficiency was calculated to be 99.73% (Fig. S2). Furthermore, inductively coupled plasma (ICP) analysis revealed that the zinc concentration in a 1 mg mL^{-1} SHK-equivalent dispersion of Zn-SHK-PEG NPs was 207.57 mg L^{-1}, which corresponds to a Zn-to-SHK molar ratio of approximately 0.91 : 1 (Table S3).

The cytocompatibility of different SHK formulations was assessed in RAW264.7 cells by CCK-8 assay (Fig. 1H). Free SHK resulted in a concentration-dependent decrease in cell viability, whereas Zn-SHK NPs showed attenuated cytotoxicity at equivalent SHK concentrations. Importantly, Zn-SHK-PEG NPs exhibited the most favorable cytocompatibility among the three formulations, with significantly higher cell viability than both free SHK and Zn-SHK NPs across most tested concentrations. These findings indicate that Zn^{2+}-assisted assembly reduced the direct cytotoxicity of SHK, and subsequent PEG modification further enhanced the cellular compatibility of the nanoparticle formulation. Consistently, the Caco-2 cell viability assay further showed that the Zn-SHK-PEG NPs exhibited improved cytocompatibility compared with free SHK and Zn-SHK NPs, particularly at higher equivalent SHK concentrations (Fig. S3). The reduced cytotoxicity of the Zn-SHK formulation may be mainly attributed to the coordination between Zn^{2+} and SHK, which enables SHK to be incorporated into the nanoparticle structure and reduces the direct exposure of cells to free SHK.[24] Further PEG modification may additionally improve the dispersion stability and overall biocompatibility of the nanoparticles, thereby contributing to the lower cytotoxicity of the final formulation.[25] Together, Zn^{2+}-mediated coordination and PEG modification improved the cellular safety of the SHK-based nanoplatform.

3.2. Oral delivery performance and inflamed intestinal retention of Zn-SHK-PEG NPs

Zn-SHK-PEG NPs maintained relatively stable hydrodynamic diameters in PBS, 10% FBS, water, simulated gastric fluid, and simulated intestinal fluid, supporting their stability under oral delivery-related conditions (Fig. S4A–D). Compared with Zn-SHK NPs, which rapidly released 80.37 ± 0.98% SHK within 2 h, the Zn-SHK-PEG NPs showed a sustained release profile, with 18.14 ± 0.63% release at 2 h and 72.85 ± 0.16% at 24 h under simulated gastrointestinal conditions (Fig. S4E). Notably, exposure to 3 mM H_2O_2 elevated the release of SHK from Zn SHK PEG NPs from 18.47 ± 0.05% to 45.03 ± 1.24% at 24 h, indicative of a release behavior responsive to oxidative inflammation (Fig. S4F). Having established their stability and controlled release behavior under oral delivery-related conditions, the *in vivo* intestinal retention of the Zn-SHK-PEG NPs was subsequently evaluated by fluorescence imaging after oral administration. The intestinal retention of Zn-SHK-PEG NPs after oral administration was evaluated using Cy5-labeled nanoparticles. As shown in Fig. 2A, *in vivo* fluorescence imaging revealed a dynamic fluorescence profile in both CON and DSS-treated mice over 24 h after oral gavage. Compared with CON mice, DSS-treated mice exhibited stronger fluorescence retention at later time points, particularly at 24 h. Quantitative analysis further confirmed significantly higher *in vivo* fluorescence intensity in DSS-treated mice at 24 h (Fig. 2C). To more accurately determine tissue distribution, major organs and the whole intestine were collected for *ex vivo* imaging at 24 h. The fluorescence signal was predominantly observed in the whole intestine, whereas relatively weak signals were detected in major organs, including the liver, heart, spleen, lungs, and kidneys (Fig. 2B). Consistently, *ex vivo* fluorescence quantification showed significantly higher whole intestine fluorescence intensity in DSS-treated mice than in CON mice (Fig. 2D). These results suggest enhanced retention of orally administered Zn-SHK-PEG NPs in the inflamed intestinal tract.

3.3. Zn-SHK-PEG NPs alleviate DSS-induced colitis

The acute colitis model was established by DSS (Fig. 3A). At the end of the experiment, the DSS group exhibited significant weight loss. SHK, Zn-SHK-PEG NPs, and 5-ASA all significantly alleviated DSS-induced body weight loss and DAI elevation compared with the DSS group (Fig. 3B and C). However, no statistically significant differences were observed among the SHK, Zn-SHK-PEG NP, and 5-ASA groups for these parameters. Relative to the CON group, the DSS treatment predominantly reduced colon length. The SHK, Zn-SHK-PEG NPs, and 5-ASA groups significantly attenuated colon shortening (Fig. 3D and E). Colonic H&E staining showed that DSS largely destroyed the crypt architecture of the mucosal layer, caused widespread epithelial cell detachment and necrosis, and produced marked inflammatory cell infiltration, while the submucosa exhibited edema and connective tissue hyperplasia. All treatments ameliorated these pathological changes to varying degrees (Fig. 3F and G). Although all treatment groups did not show statistically significant differences from each other, Zn-SHK-PEG NPs showed a consistent trend toward better therapeutic outcomes. No obvious pathological abnormalities were observed in H&E-stained sections of major organs, including the heart, liver, spleen, lungs, and kidneys, from Zn-SHK-PEG NP-treated mice compared with the CON group (Fig. S5). In addition, serum biochemical parameters, including alanine aminotransferase (ALT), aspartate aminotransferase (AST), and blood urea

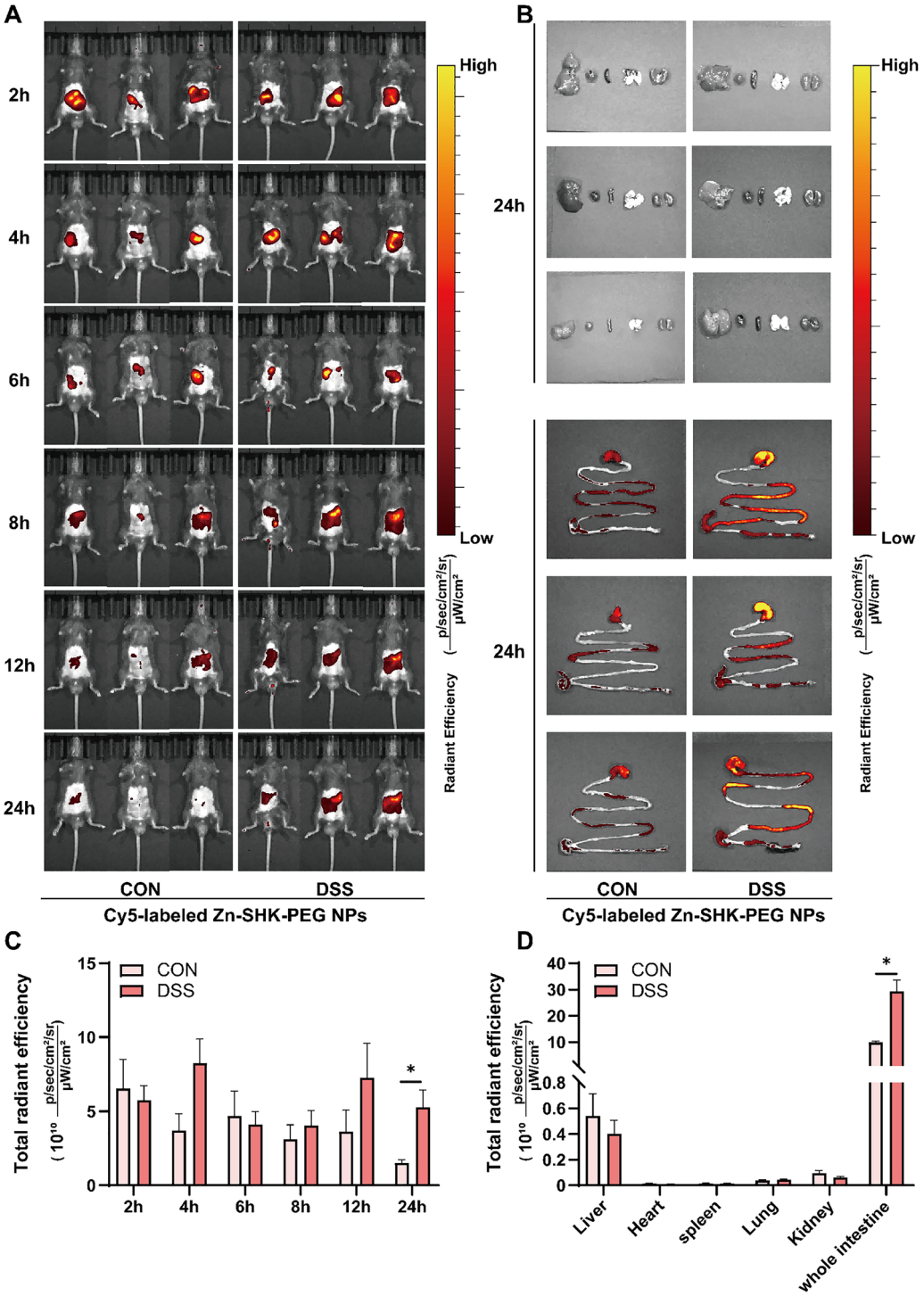

Fig. 2 *In vivo* and *ex vivo* fluorescence imaging of Cy5-labeled Zn-SHK-PEG NPs after oral administration. (A) Representative *in vivo* fluorescence images of CON and DSS-treated mice after oral gavage of Cy5-labeled Zn-SHK-PEG NPs at 2, 4, 6, 8, 12, and 24 h. (B) *Ex vivo* fluorescence images of major organs, including the heart, liver, spleen, lungs, kidneys, and intestines, collected at 24 h after administration. (C) Quantitative analysis of fluorescence intensity in the abdominal region of CON and DSS-treated mice at different time points. (D) Quantification of *ex vivo* fluorescence intensity in major organs and whole intestine at 24 h after administration. Data are presented as mean ± SD. $*p < 0.05$, $**p < 0.01$, $***p < 0.001$.

nitrogen (BUN), showed no significant differences between the CON and Zn-SHK-PEG NP-treated groups (Fig. S6). These results indicate the acceptable *in vivo* biocompatibility of Zn-SHK-PEG NPs.

3.4. Zn-SHK-PEG NPs protect the intestinal barrier and reduce inflammatory cell infiltration

Occludin and zonula occludens-1 (ZO-1) are essential in intestinal barrier function, and their abnormal expression correlates

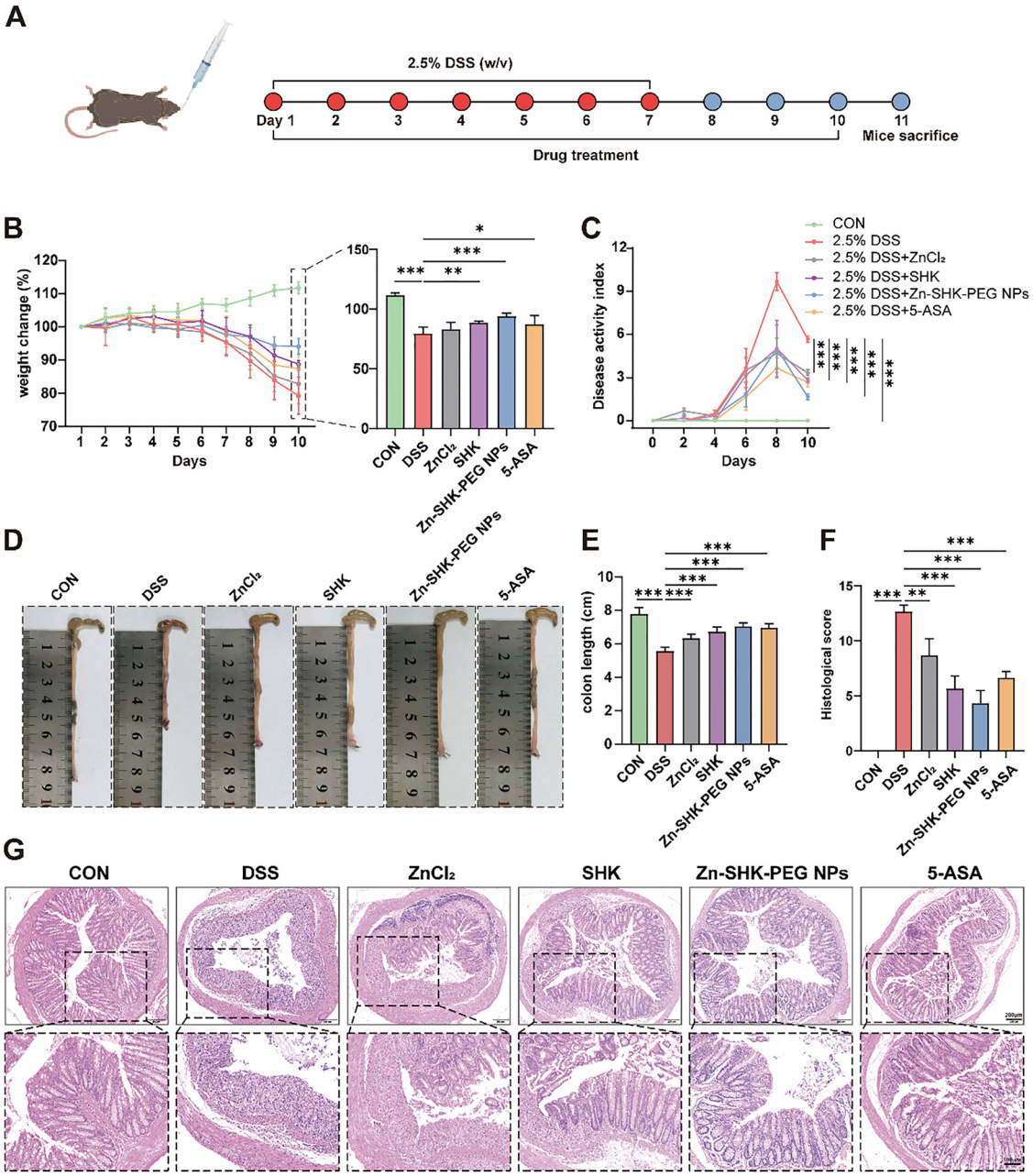

Fig. 3 Zn-SHK-PEG NPs alleviate DSS-induced colitis. (A) Experimental design of the DSS-induced colitis. (B) Daily body weight of mice. (C) Disease activity index (DAI). (D) Representative images of colon length in all groups. (E) Measurement of colon length in all groups. (F) Histopathological scores of each group. (G) Representative H&E staining images of all groups' colon tissues, with scale bars of 200 μm and 100 μm. $n = 6$, $^{*}p < 0.05$, $^{**}p < 0.01$, $^{***}p < 0.001$.

with barrier impairment.[26] Compared to the CON group, DSS treatment downregulated Occludin and ZO-1 expression. Nevertheless, treatment with $ZnCl_2$, SHK, Zn-SHK-PEG NPs, or 5-ASA restored Occludin and ZO-1 expression (Fig. 4A and B).

Excessive neutrophil infiltration and aberrant release of proinflammatory factors are hallmarks of colitis and indicate disease severity.[27] Therefore, neutrophil infiltration was assessed in the intestine by immunohistochemistry. DSS treatment markedly recruited neutrophils to inflamed colonic sites, whereas Zn-SHK-PEG NPs significantly reduced this infiltration (Fig. 4C). The anti-inflammatory effects of different treatments were evaluated by measuring serum inflammatory cytokines using ELISA. DSS treatment markedly increased the serum levels of IL-1β and IL-6 compared with the CON group, whereas $ZnCl_2$, SHK, 5-ASA, and Zn-SHK-PEG NPs significantly reduced these cytokine levels (Fig. 4D and E). Notably, compared with the SHK and $ZnCl_2$ group, Zn-SHK-PEG NPs significantly decreased serum IL-6 levels. No statistically significant differences in serum IL-1β or IL-6 levels were observed between the Zn-SHK-PEG NP and 5-ASA groups. Consistently, DSS treatment upregulated the mRNA

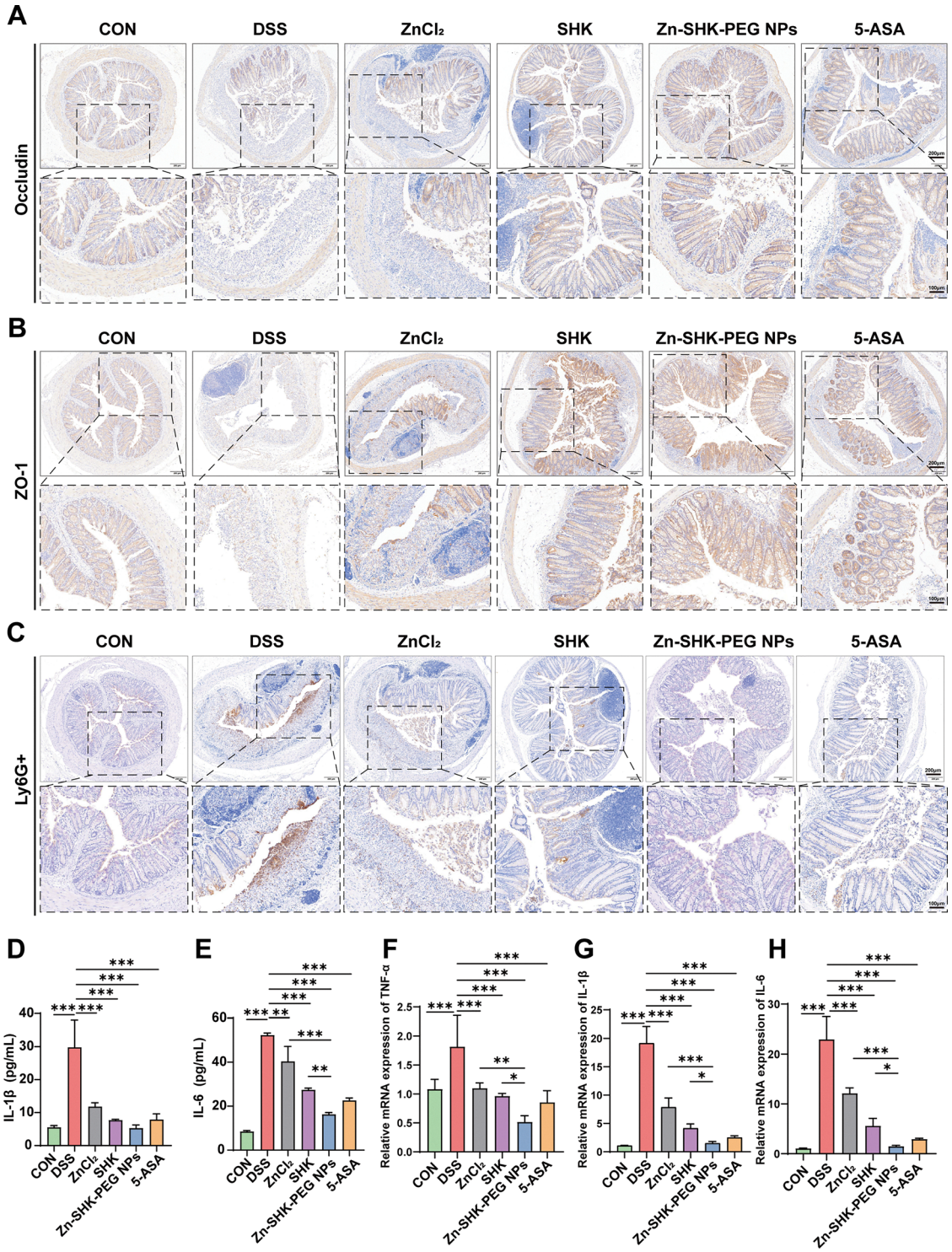

Fig. 4 Zn-SHK-PEG NPs protect the intestinal barrier and reduce inflammatory cell infiltration. (A) Representative immunohistochemical images of the ZO-1 protein in all groups, scale bars: 200 μm and 100 μm. (B) Representative immunohistochemical images of occludin protein in all groups, scale bars: 200 μm and 100 μm. (C) Representative immunohistochemical images of $Ly6G^+$ cells in each group, with scale bars of 200 μm and 100 μm. (D–E) Protein levels of IL-1β (D) and IL-6 (E) in each group, $n = 3$. (F–H) The mRNA expression of TNF-α (F), IL-1β (G), and IL-6 (H), $n = 6$. *$p < 0.05$, **$p < 0.01$, ***$p < 0.001$.

expression of pro-inflammatory cytokines in the colon, while $ZnCl_2$, SHK, 5-ASA, and Zn-SHK-PEG NPs significantly reduced the expression levels of TNF-α, IL-1β, and IL-6 (Fig. 4F–H). Compared with the SHK and $ZnCl_2$ group, Zn-SHK-PEG NPs further reduced the expression levels of these inflammatory cytokines. No statistically significant differences were observed

between the Zn-SHK-PEG NP and 5-ASA groups. These results suggested that Zn-SHK-PEG NPs exerted enhanced anti-inflammatory effects compared with free SHK and $ZnCl_2$, while showing effects comparable to 5-ASA in the regulation of inflammatory cytokines.

Zinc ions (Zn^{2+}) can suppress the production of inflammatory cytokines, thereby reducing inflammation and intestinal barrier damage.[28] However, zinc chloride ($ZnCl_2$) treatment only partially alleviated colonic inflammation, and the overall therapeutic effect remained limited. This outcome may relate to the administration route, dose, or other parameters. By contrast, SHK demonstrated superior biological effects in restoring barrier function and suppressing inflammation, suggesting that the therapeutic benefit of Zn-SHK-PEG NPs derives chiefly from the SHK component, with Zn^{2+} providing a synergistic anti-inflammatory contribution. In addition, the three-dimensional network formed by metal–polyphenol coordination between Zn^{2+} and SHK markedly improves drug solubility and bioavailability,[19,29] which together enhance the overall therapeutic outcome.

3.5. Zn-SHK-PEG NPs reduce histamine levels in colitis mice associated with decreased HDC expression in macrophages

The regulation of intestinal inflammatory processes is significantly influenced by histamine.[30] Elevated histamine levels were observed in patients with ulcerative colitis relative to healthy control subjects.[31] Serum ELISA showed that serum histamine was predominantly elevated in the DSS group. Treatment with Zn-SHK-PEG NPs markedly reduced histamine levels (Fig. 5A). Abnormal histamine accumulation is linked to dysregulation of its metabolic enzymes.[32] Histamine production is primarily controlled by histidine decarboxylase (HDC), while for its degradation, histamine *N*-methyltransferase (HNMT) serves as the predominant enzyme, utilizing histamine as its only substrate.[33] Although HNMT protein expression did not show a significant intergroup difference, a substantial upregulation of HDC was detected in the DSS-treated mice relative to controls (Fig. 5B and C). Given the established involvement of COX-2 in inflammatory responses associated with colitis, colonic COX-2 expression was further examined.[34] Zn-SHK-PEG NPs significantly reduced DSS-induced HDC expression and COX-2 expression (Fig. 5D and E). The elevated COX-2 level in colonic tissues further reflected the inflammatory state induced by DSS, and its reduction after Zn-SHK-PEG NPs treatment was broadly consistent with previous findings describing the anti-inflammatory activity of shikonin in colitis related models.[35,36]

To explore the potential cellular source associated with elevated HDC in DSS colitis, we first assessed whether DSS challenge was accompanied by obvious mast cell accumulation, as mast cells are classical histamine-producing cells.[33] Toluidine blue staining and immunohistochemical analysis of tryptase and CD117 showed that mast cell numbers in colonic tissues were not obviously increased in DSS-treated mice compared with controls (Fig. 5F). These observations suggested that the elevated histamine level in this model may not be primarily explained by increased mast cell infiltration. We therefore further examined the spatial relationship between HDC and macrophages, given the established role of macrophages in DSS colitis and their capacity to express HDC.[37] Immunofluorescence analysis showed that HDC was mainly distributed in areas enriched for $F4/80^+$ macrophages (Fig. 5G). Recent evidence has shown that histamine produced by macrophages is pivotal for driving angiogenesis in inflammatory granulation tissue.[38] Combined with the pronounced spatial colocalization of HDC and macrophages observed in this study, macrophages are implicated by these data as potential contributors of histamine in inflammatory tissue.

3.6. Zn-SHK-PEG NPs alleviate macrophage inflammatory responses involving PKM2-associated HDC regulation

To determine whether Zn-SHK-PEG NPs exert their anti-inflammatory and immunomodulatory effects *via* HDC, RAW264.7 cells were stimulated with LPS. Zn-SHK-PEG NPs markedly suppressed LPS-induced HDC expression and COX-2 protein levels (Fig. 6A–C). Zn-SHK-PEG NPs significantly reduced the LPS-driven increase in IL-1β mRNA. Compared with the free SHK group, Zn-SHK-PEG NPs produced a significantly greater reduction in HDC protein expression, indicating that the nanoparticle formulation enhanced the inhibitory effect of SHK on HDC under inflammatory stimulation (Fig. 6D). Notably, exogenous histamine induced upregulation of IL-1β mRNA in RAW264.7 cells (Fig. 6E). To clarify the role of HDC in the anti-inflammatory response, HDC was knocked down by small interfering RNA (siRNA) and confirmed the knockdown efficiency by RT-qPCR. Based on the comparative effects observed for free SHK and Zn-SHK-PEG NPs in LPS-stimulated macrophages, subsequent siRNA experiments were performed using Zn-SHK-PEG NPs to further investigate the mechanism of the nanoparticle formulation. Compared with the LPS-treated group, si-HDC predominantly suppressed the LPS-induced increase in IL-1β mRNA and markedly reduced COX-2 protein expression. Furthermore, combined treatment with si-HDC and Zn-SHK-PEG NPs produced an additional reduction in COX-2 and IL-1β levels (Fig. 6F-I). In LPS stimulated RAW264.7 macrophages, the Zn-SHK-PEG NPs decreased HDC, COX-2, and IL-1β expression. Among these changes, the reductions in COX-2 and IL-1β directly reflected the suppression of inflammatory responses. Notably, si-HDC reduced COX-2 at the protein level and suppressed IL-1β expression at the mRNA level, suggesting that the HDC/histamine axis is associated with the regulation of inflammatory responses. This possibility is in line with previous studies linking histamine signaling to increased COX-2 expression in multiple cell types.[39,40] Since the anti-inflammatory effect was attenuated but not completely abolished after HDC knockdown, HDC appears to be an important contributor, but not the sole mediator, of the inhibitory effect of Zn-SHK-PEG NPs. This is consistent with the typical multi-target activity of traditional Chinese medicine monomers.[41]

Previous studies have established SHK as a natural inhibitor of PKM2,[42] and the present study showed that Zn-SHK-PEG NPs were also associated with modulation of HDC expression.

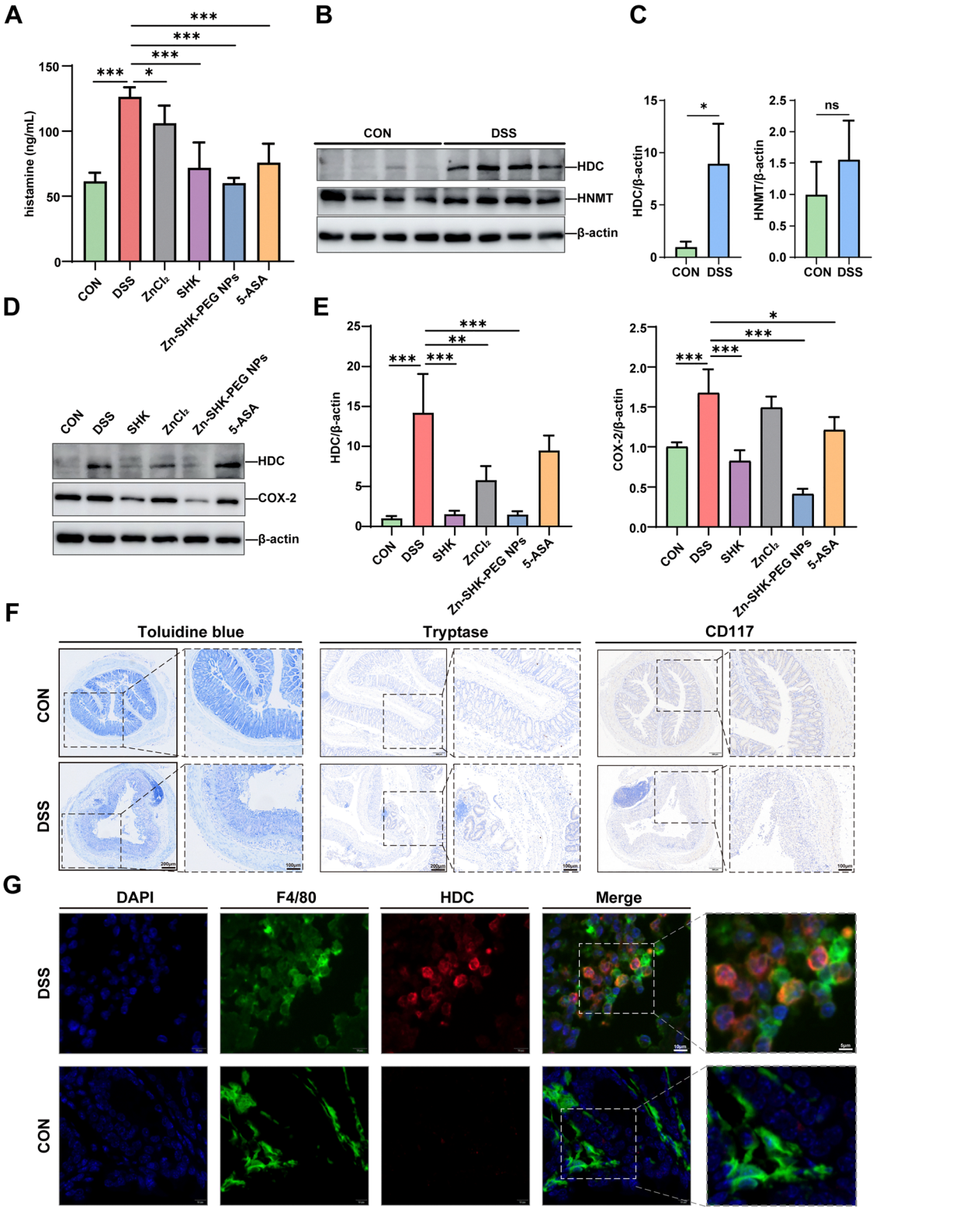

Fig. 5 Zn-SHK-PEG NPs reduce HDC expression in DSS-induced colitis mice. (A) Serum histamine concentrations were measured by ELISA. (B) Western blotting of HDC and HNMT protein levels between the CON and DSS groups. (C) Quantification of HDC and HNMT protein level in CON and DSS groups. (D) Western blotting of HDC and COX-2 protein levels across all groups. (E) Quantification of HDC and COX-2 protein expression across all groups. (F) Representative images of colon tissue from the CON and DSS groups stained with toluidine blue, trypsin-like protease, and CD117 immunohistochemistry, with scale bars of 200 μm and 100 μm. (G) Typical images showing co-localization of F4/80 and HDC by immunofluorescence, with scale bars of 10 μm and 5 μm. Experiments were repeated three times. *$p < 0.05$, **$p < 0.01$, and ***$p < 0.001$.

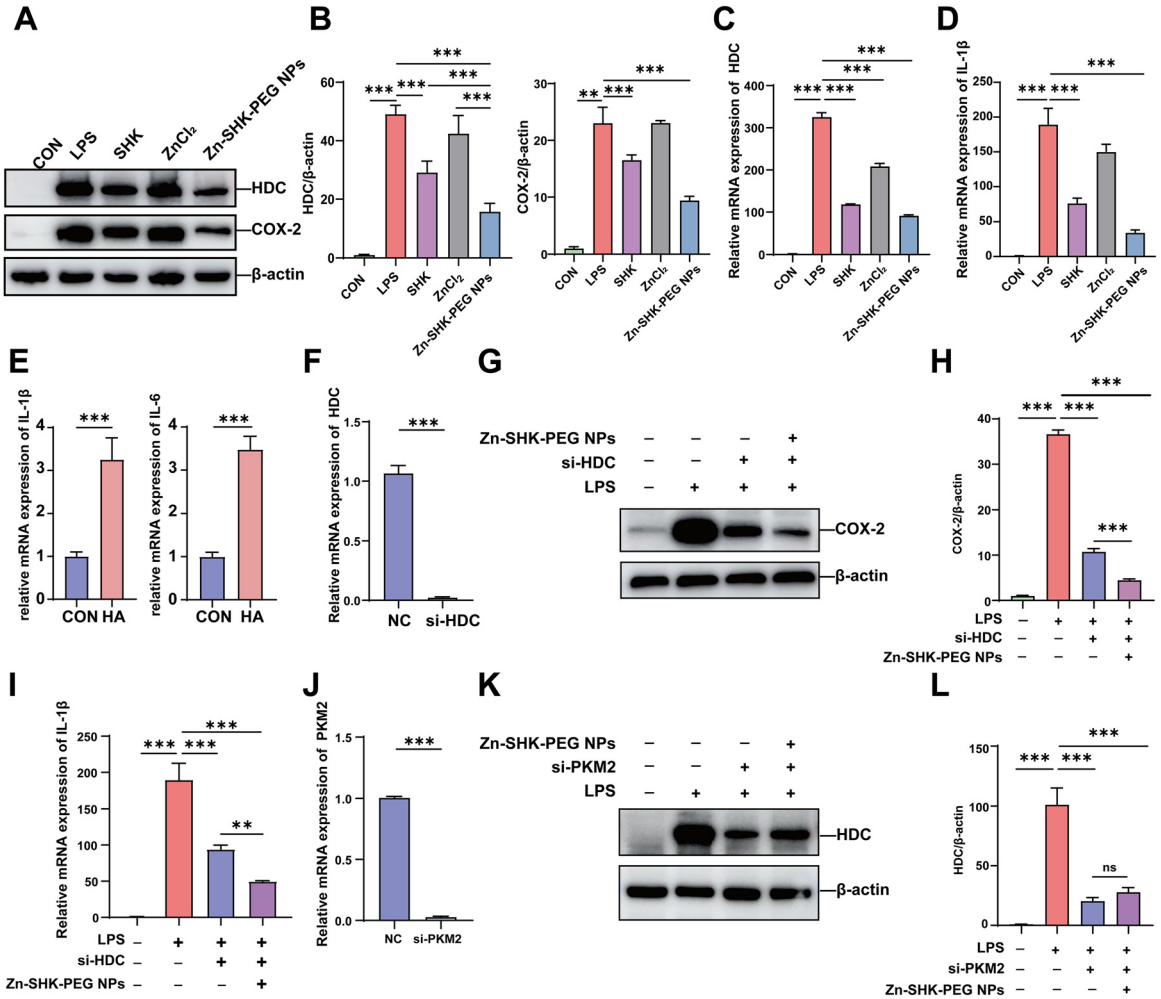

Fig. 6 Zn-SHK-PEG NPs alleviate macrophage inflammatory responses involving PKM2-dependent HDC regulation. (A) Western blot assessment of HDC and COX-2 protein levels. (B) Quantification of HDC and COX-2 protein expression, $n = 5$. (C) HDC mRNA expression levels across groups. (D) IL-1β mRNA expression across groups. (E) IL-1β and IL-6 mRNA expression after 400 μM histamine stimulation. (F) RT-qPCR validation of HDC knockdown efficiency. (G) Western blot assessment of the COX-2 protein level. (H) Quantification of COX-2 protein expression. (I) RT-qPCR assessment of the effect of si-HDC on IL-1β mRNA expression. (J) RT-qPCR validation of PKM2 knockdown efficiency. (K) Western blot assessment of the HDC protein level. (L) Quantification of HDC protein expression. $n = 3$, $^{*}p < 0.05$, $^{**}p < 0.01$, and $^{***}p < 0.001$.

To test whether HDC constitutes an anti-inflammatory pathway independent of PKM2, we knocked down PKM2. In LPS-stimulated RAW264.7 macrophages, si-PKM2 attenuated LPS-induced HDC expression at both the mRNA and protein levels. Under these conditions, Zn-SHK-PEG NPs did not produce any further inhibitory effect (Fig. 6J–L). These findings suggest that PKM2 may be involved in the regulation of the HDC histamine axis. However, the present study does not directly demonstrate transcriptional regulation of HDC by PKM2. Further studies, such as PKM2 transcriptional activity assays, promoter analysis, or mutant-based validation, are required to confirm the precise mechanism by which PKM2 regulates HDC expression.

3.7. Zn-SHK-PEG NPs do not alter the abundance of HDC in the gut microbiota

Gut microbiota can also promote colitis by increasing histamine levels.[43] To investigate this, mouse fecal samples were collected for metagenomic analysis. A Venn diagram showed 6149 species shared among the three groups (Fig. 7A). Assessment of α diversity revealed that species richness was comparable across the CON, DSS, and Zn-SHK-PEG NPs treatment groups measured by the Ace and Chao indices (Fig. 7B and C). This has been observed in several animal studies and may reflect expansion of opportunistic pathogenic taxa.[44,45] Analysis using both the Simpson and Shannon indices revealed that the DSS-treated mice exhibited increased gut microbiome diversity compared to controls (Fig. 7D and E). Employing β diversity metrics including principal coordinates analysis (PCoA), non-metric multidimensional scaling (NMDS), and analysis of similarities (ANOSIM), distinct gut microbial compositions were discerned among the CON, DSS and Zn-SHK-PEG NP groups ($p < 0.05$) (Fig. 7F–H). Based on KEGG annotations, differential abundance analyses of glycolysis and histidine metabolism were performed. Visualization revealed

no significant differences in pyruvate kinase (PK) or HDC abundance among the CON, DSS and Zn-SHK-PEG NPs groups (Fig. 7I and J). These findings suggest that Zn-SHK-PEG NPs do not significantly alter HDC expression at the gut microbiota level.

3.8. Zn-SHK-PEG NPs upregulate the abundance of *Akkermansia muciniphila* and improve the inflammatory microenvironment

Phylsum-level analysis and species-level analysis revealed DSS-induced dysbiosis, characterized by reduced *Bacteroidota*,

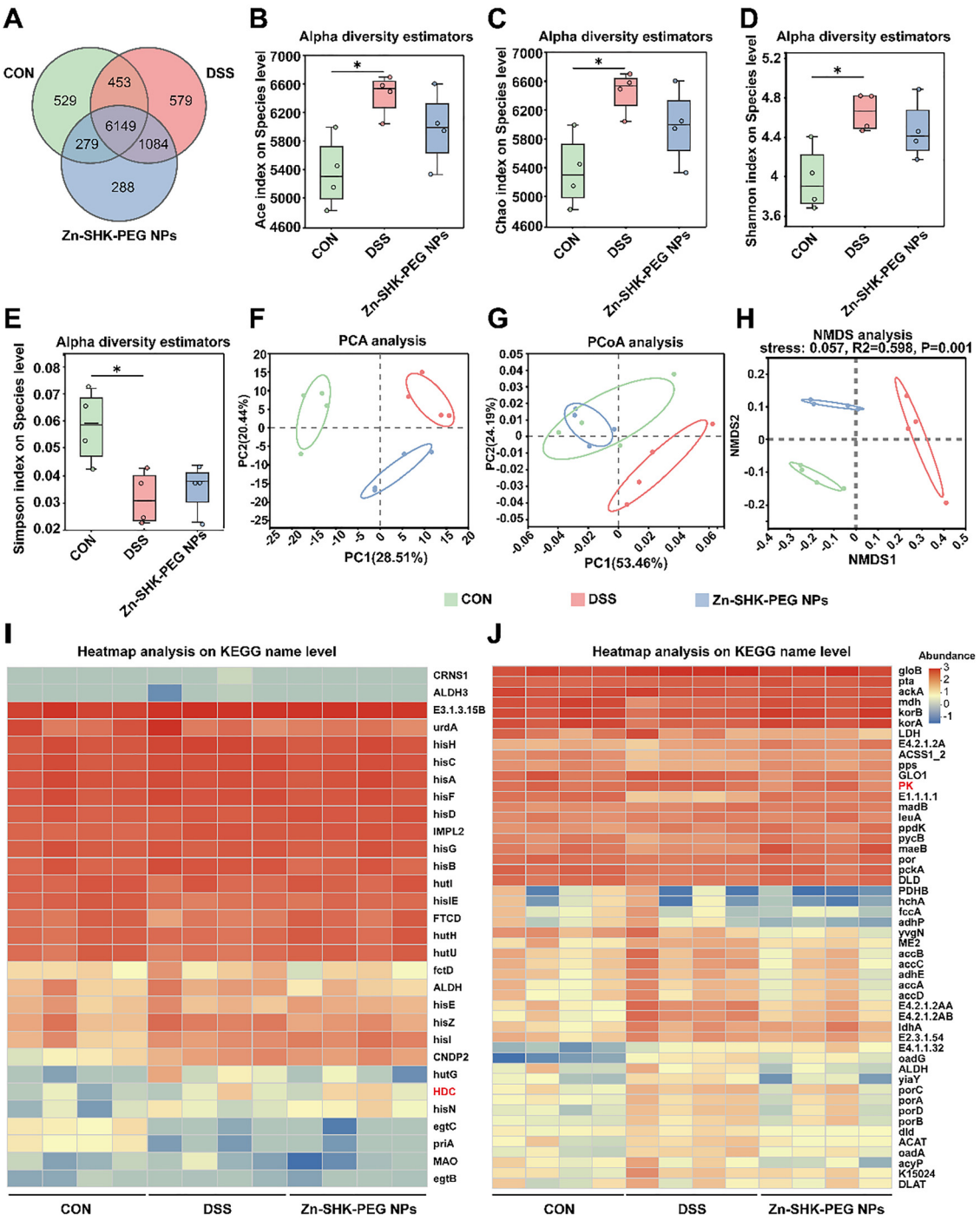

Fig. 7 Zn-SHK-PEG NPs attenuated DSS-induced gut microbiota dysbiosis. (A) Venn diagram comparing the CON, DSS, and Zn-SHK-PEG NPs groups. (B–E) Alpha diversity analysis (Ace, Chao, Shannon, Simpson) for the CON, DSS, and Zn-SHK-PEG NPs groups. (F) PCA of the CON, DSS, and Zn-SHK-PEG NPs groups. (G) PCoA of the CON, DSS, and Zn-SHK-PEG NPs groups. (H) NMDS of the CON, DSS, and Zn-SHK-PEG NPs groups. (I and J) Relative abundance changes in histidine metabolism and glycolysis pathways based on KEGG annotation. $n = 4$, $^{*}p < 0.05$, $^{**}p < 0.01$, $^{***}p < 0.001$.

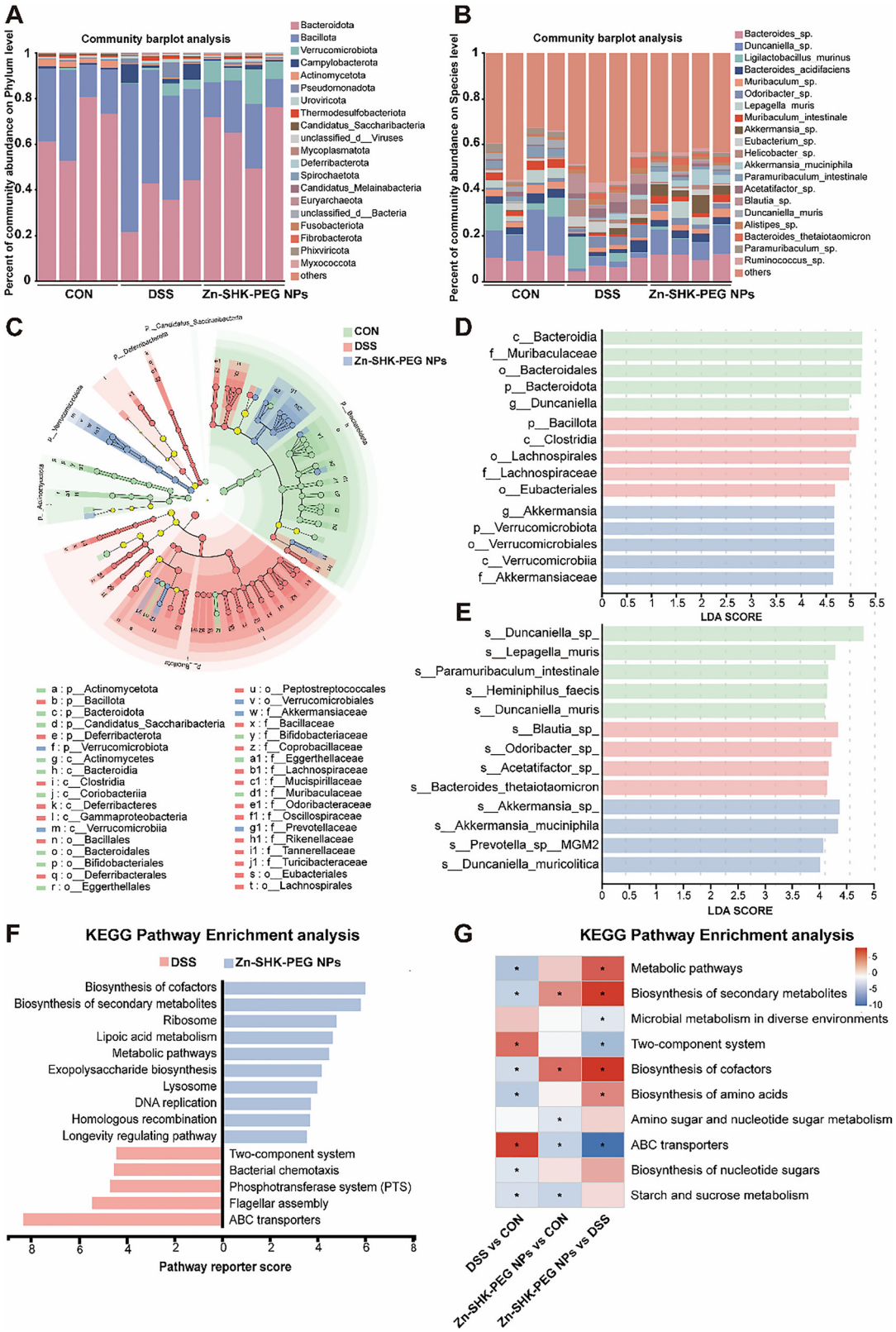

Fig. 8 Zn-SHK-PEG NPs markedly increased *Akkermansia* abundance and ameliorated colitis. (A) At the phylum level, relative abundance of microbiota in the CON, DSS, and Zn-SHK-PEG NPs groups. (B) At the species level, relative abundances of microbiota in the CON, DSS, and Zn-SHK-PEG NPs groups. (C) LEfSe differential-discriminant analysis visualization (LDA > 3.5). (D) Dominant taxa per group (LDA > 4, top 5 by abundance). (E) Dominant taxa at the species level per group (LDA > 4). (F) KEGG pathway enrichment between the DSS and Zn-SHK-PEG NPs groups (|Reporter score| ≥ 2, top 15 differential pathways). (G) KEGG pathway enrichment among the CON, DSS, and Zn-SHK-PEG NPs groups (|Reporter score| ≥ 2, top 10 differential pathways). $n = 4$, $^{*}p < 0.05$, $^{**}p < 0.01$, and $^{***}p < 0.001$.

Duncaniella sp. and enriched *Bacillota* and *Akkermansia muciniphila* compared to controls (Fig. 8A and B). This shift was restored by Zn-SHK-PEG NPs treatment, which also notably enriched *Verrucomicrobiota*. At the species level, the NPs concurrently elevated the diminished populations of *Duncaniella* sp. and *Akkermansia muciniphila*.

Differential abundance was determined using LEfSe (linear discriminant analysis effect size), with taxa meeting an LDA threshold >4 and the top five in abundance selected for display (Fig. 8C and D). The CON group showed enrichment in the class *Bacteroidia*, family *Muribaculaceae*, and order *Bacteroidales*. In contrast, the DSS group featured a predominance of the phylum *Bacillota* and class Clostridia, a pattern aligning with reports of a transient increase and subsequent decline in gut microbiota during DSS exposure.[46] Conversely, Zn-SHK-PEG NPs treatment markedly increased the relative abundance of the genus *Akkermansia*, phylum *Verrucomicrobiota*, and order *Verrucomicrobiales*.

To further define the dominant taxa in each group, species with LDA scores $>$ 4 were visualized. In the CON group, the dominant taxa were *Duncaniella* sp., *Lepagella muris*, and *Paramuribaculum intestinale*. In the DSS group, dominance was mainly limited to taxa identified only at the genus level, including *Blautia* sp., *Odoribacter* sp., *Acetatifactor* sp., and *Bacteroides thetaiotaomicron*. The Zn-SHK-PEG NPs group was dominated by *Akkermansia* sp., *Akkermansia muciniphila*, *Prevotella* sp. *MGM2*, and *Duncaniella muricolitica* (Fig. 8E). In the DSS-enriched fraction, several dominant bacteria remain unclassified. Some studies report an increase in Blautia in UC patients.[47] Acetatifactor has been reported to possess potential proinflammatory effects.[48] Notably, different species and even strains can exhibit heterogeneity, and their impacts on the host require further investigation.[49] The microbial community in the Zn-SHK-PEG NPs group showed marked enrichment in the *Akkermansia*, with a consistent enrichment trend from phylum to species levels, indicating that *Akkermansia*-related taxa dominate this group's microbiota. *Akkermansia muciniphila* can restore mucus layer integrity and can reduce proinflammatory cytokine release, thereby alleviating DSS-induced colitis.[50,51] Thus, although Zn-SHK-PEG NPs did not affect HDC abundance at the gut microbiota level, they promoted mucosal barrier repair and improved the inflammatory microenvironment *via* increasing the abundance of genus *Akkermansia*.

KEGG pathway enrichment analysis showed that the DSS group was significantly enriched for ABC transporters, flagellar assembly, and bacterial chemotaxis. Studies indicate that potential pathogens can enhance the transport of glucose and amino acids through ABC transporter systems, thereby promoting their colonization in favorable environments.[52] After treatment with Zn-SHK-PEG NPs, enrichment shifted mainly to pathways related to cofactor biosynthesis, secondary metabolite biosynthesis, ribosomes, lipoic acid metabolism, metabolic pathways, and extracellular polysaccharide biosynthesis (Fig. 8F and G). Previous studies have shown that cofactors, such as NAD^+, were associated with protective effects in DSS-induced colitis and the maintenance of gut homeostasis.[53] Lipoic acid is one of the cofactors, as previous studies have shown that lipoic acid-related pathways are enriched in beneficial gut bacteria.[54] A previous study suggested that fermented tea may alleviate colitis by restoring gut microbiota and modulating host metabolic pathways, particularly secondary metabolite biosynthesis, which may be associated with its anti-inflammatory effects.[55] It should be noted that the metagenomic sequencing analysis was performed with a relatively limited sample size (n = 4 per group), and therefore these microbiome results should be interpreted as exploratory. Further studies with larger cohorts and targeted microbial validation are required to confirm the contribution of gut microbiota remodeling to the therapeutic effects of Zn-SHK-PEG NPs.

4. Conclusion

In summary, Zn-SHK-PEG NPs were developed as a Zn^{2+}-assisted SHK self-assembled nanomedicine stabilized by PEG modification. The formulation achieved efficient SHK incorporation, improved cytocompatibility, stability in physiological and gastrointestinal media, sustained SHK release, oxidation-responsive release, and enhanced retention in inflamed intestine after oral administration. Zn-SHK-PEG NPs alleviated DSS-induced colitis. The therapeutic effects involved suppression of inflammatory responses, regulation of the HDC/histamine axis, protection of the epithelial barrier, and modulation of gut microbiota. These results suggest that Zn-SHK-PEG NPs may serve as a potential SHK-based oral nanomedicine strategy for ulcerative colitis treatment.

Author contributions

Wang Zhang: conceptualization; investigation; data curation; formal analysis; writing – original draft. Jingrou Sun: investigation; data curation; formal analysis. Ying Ou: investigation; data curation. Jing Zhang: investigation; data curation. Yilan Bai: investigation; data curation. Jingxi Hong: investigation; data curation. Lingchang Meng: methodology; resources. Yi Song: methodology; resources. Tiepeng Wang: methodology; resources. Zhiting Sun: project administration; supervision; writing – review and editing. Jing Wu: conceptualization; funding acquisition; supervision; project administration; writing – review and editing.

Conflicts of interest

The authors declare that they have no known competing financial interests or personal relationships that could have appeared to influence the work reported in this paper.

Data availability

Data will be made available on request. The supplementary information (SI) includes additional experimental details,

characterization data of Zn-SHK-PEG NPs, supporting experimental results, and supplementary figures and tables related to this study. See DOI: https://doi.org/10.1039/d6tb00517a.

Acknowledgements

This study was funded by the National Natural Science Foundation of China (81873160); Nanjing Drum Tower Hospital Senior Talents Projects; The Project of Institute of Chinese Medicine, Nanjing University (ICM2024004); The Aid Project of Nanjing Drum Tower Hospital Health, Education & Research Foundation; Nanjing Health Science and Technology Development Foundation (YKK23090), and the Project of the Institute of Chinese Medicine, Nanjing University (ICM2024027).

References

1 R. Ungaro, S. Mehandru, P. B. Allen, L. Peyrin-Biroulet and J.-F. Colombel, Ulcerative colitis, *Lancet*, 2017, **389**, 1756–1770, DOI: 10.1016/S0140-6736(16)32126-2.

2 S. Honap, V. Jairath, S. Danese and L. Peyrin-Biroulet, Navigating the complexities of drug development for inflammatory bowel disease, *Nat. Rev. Drug Discovery*, 2024, **23**, 546–562, DOI: 10.1038/s41573-024-00953-0.

3 C. L. Berre, S. Honap and L. Peyrin-Biroulet, Ulcerative colitis, *Lancet*, 2023, **402**, 571–584, DOI: 10.1016/S0140-6736(23)00966-2.

4 G. G. Kaplan and J. W. Windsor, The four epidemiological stages in the global evolution of inflammatory bowel disease, *Nat. Rev. Gastroenterol. Hepatol.*, 2021, **18**, 56–66, DOI: 10.1038/s41575-020-00360-x.

5 S. Vieujean, V. Jairath, L. Peyrin-Biroulet, M. Dubinsky, M. Iacucci, F. Magro and S. Danese, Understanding the therapeutic toolkit for inflammatory bowel disease, *Nat. Rev. Gastroenterol. Hepatol.*, 2025, **22**, 371–394, DOI: 10.1038/s41575-024-01035-7.

6 A. Salas, C. Hernandez-Rocha, M. Duijvestein, W. Faubion, D. McGovern, S. Vermeire, S. Vetrano and N. Vande Casteele, JAK-STAT pathway targeting for the treatment of inflammatory bowel disease, *Nat. Rev. Gastroenterol. Hepatol.*, 2020, **17**, 323–337, DOI: 10.1038/s41575-020-0273-0.

7 W. J. Sandborn, B. G. Feagan, G. D'Haens, D. C. Wolf, I. Jovanovic, S. B. Hanauer, S. Ghosh, A. Petersen, S. Y. Hua, J. H. Lee, L. Charles, D. Chitkara, K. Usiskin, J.-F. Colombel, L. Laine and S. Danese, Ozanimod as induction and maintenance therapy for ulcerative colitis, *N. Engl. J. Med.*, 2021, **385**, 1280–1291, DOI: 10.1056/NEJMoa2033617.

8 B. E. Sands, B. G. Feagan, L. Peyrin-Biroulet, S. Danese, D. T. Rubin, O. Laurent, A. Luo, D. D. Nguyen, J. Lu, M. Yen, J. Leszczyszyn, R. Kempiński, D. P. B. McGovern, C. Ma, T. E. Ritter and S. Targan, ARTEMIS-UC Study Group, Phase 2 trial of anti-TL1A monoclonal antibody tulisokibart for ulcerative colitis, *N. Engl. J. Med.*, 2024, **391**, 1119–1129, DOI: 10.1056/NEJMoa2314076.

9 Y. Gvozdeva and R. Staynova, pH-dependent drug delivery systems for ulcerative colitis treatment, *Pharmaceutics*, 2025, **17**, 226, DOI: 10.3390/pharmaceutics17020226.

10 P. Núñez F, R. Quera, C. Bay, F. Castro and G. Mezzano, Drug-induced liver injury used in the treatment of inflammatory bowel disease, *J. Crohns Colitis*, 2022, **16**, 1168–1176, DOI: 10.1093/ecco-jcc/jjac013.

11 M. Rihan and S. S. Sharma, Inhibition of pyruvate kinase M2 (PKM2) by shikonin attenuates isoproterenol-induced acute myocardial infarction *via* reduction in inflammation, hypoxia, apoptosis, and fibrosis, *Naunyn Schmiedebergs Arch. Pharmacol.*, 2024, **397**, 145–159, DOI: 10.1007/s00210-023-02593-4.

12 B. Lohberger, H. Kaltenegger, N. Eck, D. Glänzer, P. Sadoghi, A. Leithner, R. Bauer, N. Kretschmer and B. Steinecker-Frohnwieser, Shikonin derivatives inhibit inflammation processes and modulate MAPK signaling in human healthy and osteoarthritis chondrocytes, *Int. J. Mol. Sci.*, 2022, **23**, 3396, DOI: 10.3390/ijms23063396.

13 X.-H. Wang, C.-P. Shen, T.-T. Wang, Y. Huang, Y. Jin, M.-Y. Zhou, M.-Y. Zhang, S.-L. Gu, M.-Q. Wang, Z.-C. Liu, R. Li and L. Cai, Shikonin suppresses rheumatoid arthritis by inducing apoptosis and autophagy *via* modulation of the AMPK/mTOR/ULK-1 signaling pathway, *Phytomedicine*, 2024, **128**, 155512, DOI: 10.1016/j.phymed.2024.155512.

14 Y. Liang, D. Ju, W. Liu, D. Wu, Y. Zhao, Y. Du, X. Li and M. Zhao, Natural shikonin potentially alters intestinal flora to alleviate acute inflammation, *Microorganisms*, 2023, **11**, 2139, DOI: 10.3390/microorganisms11092139.

15 J. Hu, K. Feng, Y. Cong, X. Li, Y. Jiang, X. Jiao, Y. Li, Y. Zhang, X. Dong, W. Lu, Z. Ding and H. Hong, Nanosized shikonin-Fe(III) coordination material for synergistic wound treatment: an initial explorative study, *ACS Appl. Mater. Interfaces*, 2022, **14**, 56510–56524, DOI: 10.1021/acsami.2c16011.

16 D. Li, Q. Wu, C. Long, P. Yi, S. Wang, Q. Wang and W. Teng, Hybrid-designed metal-phenolic nanoparticles for synergistic nano-gene periodontal therapy, *Biomaterials*, 2025, **322**, 123417, DOI: 10.1016/j.biomaterials.2025.123417.

17 Q. Hu, C. Wu, L. Wang, D. Cao, J. Wang, Y. Du, M. Liu and K. Li, Multifunctional metal–phenolic nanoparticles with antibacterial and anti-inflammatory effects for osteomyelitis management, *J. Mater. Chem. B*, 2025, **13**, 3067–3079, DOI: 10.1039/D4TB02649G.

18 D. Liang, X. Shen, L. Han, H. Ren, T. Zang, L. Tan, Z. Lu, X. Liao, B. S. S. Vetha, Y. Liu, C. Zhang and J. Sun, Dual-ROS sensitive moieties conjugate inhibits curcumin oxidative degradation for colitis precise therapy, *Adv Healthc Mater*, 2024, **13**, e2303016, DOI: 10.1002/adhm.202303016.

19 J. Jin, X. Ye, Z. Huang, S. Jiang and D. Lin, Curcumin@Fe/tannic acid complex nanoparticles for inflammatory bowel disease treatment, *ACS Omega*, 2024, **9**, 14316–14322, DOI: 10.1021/acsomega.3c10214.

20 H. He, Q. Qin, F. Xu, Y. Chen, S. Rao, C. Wang, X. Jiang, X. Lu and C. Xie, Oral polyphenol-armored nanomedicine for targeted modulation of gut microbiota-brain

interactions in colitis, *Sci. Adv.*, 2023, **9**, eadf3887, DOI: 10.1126/sciadv.adf3887.

21 J. Li, J. Song, Z. Deng, J. Yang, X. Wang, B. Gao, Y. Zhu, M. Yang, D. Long, X. Luo, M. Zhang, M. Zhang and R. Li, Robust reactive oxygen species modulator hitchhiking yeast microcapsules for colitis alleviation by trilogically intestinal microenvironment renovation, *Bioact. Mater.*, 2024, **36**, 203–220, DOI: 10.1016/j.bioactmat.2024.02.033.

22 J. Yang, X. Xia, M. Du, S. Cheng, B. Zhu and X. Xu, Highly effective nobiletin-MPN in yeast microcapsules for targeted modulation of oxidative stress, NLRP3 inflammasome activation, and immune responses in ulcerative colitis, *J. Agric. Food Chem.*, 2024, **72**, 13054–13068, DOI: 10.1021/acs.jafc.3c09530.

23 E. Donadoni, P. Siani, S. Gambari, D. Campi, G. Frigerio and C. Di Valentin, Optimizing polyethylene glycol coating for stealth nanodiamonds, *ACS Appl. Mater. Interfaces*, 2025, **17**, 19304–19316, DOI: 10.1021/acsami.4c21303.

24 J. Guo, Y. Miao, F. Nie, F. Gao, H. Li, Y. Wang, Q. Liu, T. Zhang, X. Yang, L. Liu, H. Fan, Q. Wang and H. Qiao, Zn-shik-PEG nanoparticles alleviate inflammation and multi-organ damage in sepsis, *J. Nanobiotechnol.*, 2023, **21**, 448, DOI: 10.1186/s12951-023-02224-3.

25 M. Yu, S. Huang, K. J. Yu and A. M. Clyne, Dextran and polymer polyethylene glycol (PEG) coating reduce both 5 and 30 nm iron oxide nanoparticle cytotoxicity in 2D and 3D cell culture, *Int. J. Mol. Sci.*, 2012, **13**, 5554–5570, DOI: 10.3390/ijms13055554.

26 J. Mo, J. Ni, M. Zhang, Y. Xu, Y. Li, N. Karim and W. Chen, Mulberry anthocyanins ameliorate DSS-induced ulcerative colitis by improving intestinal barrier function and modulating gut microbiota, *Antioxidants*, 2022, **11**, 1674, DOI: 10.3390/antiox11091674.

27 M. Ortega-Zapero, R. Gomez-Bris, I. Pascual-Laguna, A. Saez and J. M. Gonzalez-Granado, Neutrophils and NETs in pathophysiology and treatment of inflammatory bowel disease, *Int. J. Mol. Sci.*, 2025, **26**, 7098, DOI: 10.3390/ijms26157098.

28 C. Xiao, L. Comer, X. Pan, N. Everaert, M. Schroyen and Z. Song, Zinc glycinate alleviates LPS-induced inflammation and intestinal barrier disruption in chicken embryos by regulating zinc homeostasis and TLR4/NF-κB pathway, *Ecotoxicol. Environ. Saf.*, 2024, **272**, 116111, DOI: 10.1016/j.ecoenv.2024.116111.

29 Z. Xu, H. Yu, Z. Hu, C. Wang, Z. Song, D. Cai, B. Ma, H. Ge, J.-B. Fan, Y. Zhu and W. Cheng, A zinc-loureirin B coordination nanozyme for oxidative and inflammatory microenvironment remodeling in osteoarthritis, *ACS Appl. Mater. Interfaces*, 2025, **17**, 50203–50216, DOI: 10.1021/acsami.5c07574.

30 K. A. Dvornikova, O. N. Platonova and E. Y. Bystrova, Inflammatory Bowel Disease: Crosstalk between Histamine, Immunity, and Disease, *Int. J. Mol. Sci.*, 2023, **24**, 9937, DOI: 10.3390/ijms24129937.

31 D. Neumann and R. Seifert, The therapeutic potential of histamine receptor ligands in inflammatory bowel disease, *Biochem. Pharmacol.*, 2014, **91**, 12–17, DOI: 10.1016/j.bcp.2014.06.004.

32 D. Kanta, E. Katsamakas, A. M. B. Gudiksen and M. Jalili, Histamine metabolism in IBD: towards precision nutrition, *Nutrients*, 2025, **17**, 2473, DOI: 10.3390/nu17152473.

33 S. Heidarzadeh-Asl, M. Maurer, A. Kiani, D. Atiakshin, P. Stahl Skov and D. Elieh-Ali-Komi, Novel insights on the biology and immunologic effects of histamine: a road map for allergists and mast cell biologists, *J. Allergy Clin. Immunol.*, 2025, **155**, 1095–1114, DOI: 10.1016/j.jaci.2024.12.1081.

34 M. Fukata, A. Chen, A. Klepper, S. Krishnareddy, A. S. Vamadevan, L. S. Thomas, R. Xu, H. Inoue, M. Arditi, A. J. Dannenberg and M. T. Abreu, Cox-2 is regulated by toll-like receptor-4 (TLR4) signaling and is important for proliferation and apoptosis in response to intestinal mucosal injury, *Gastroenterology*, 2006, **131**, 862–877, DOI: 10.1053/j.gastro.2006.06.017.

35 H. Han, W. Sun, L. Feng, Z. Wen, M. Yang, Y. Ma, J. Fu, X. Ma, X. Xu, Z. Wang, T. Yin, X.-M. Wang, G.-H. Lu, J.-L. Qi, H. Lin and Y. Yang, Differential relieving effects of shikonin and its derivatives on inflammation and mucosal barrier damage caused by ulcerative colitis, *PeerJ*, 2021, **9**, e10675, DOI: 10.7717/peerj.10675.

36 M. Vacca, I. Kamzolas, L. M. Harder, F. Oakley, C. Trautwein, M. Hatting, T. Ross, B. Bernardo, A. Oldenburger, S. T. Hjuler, I. Ksiazek, D. Lindén, D. Schuppan, S. Rodriguez-Cuenca, M. M. Tonini, T. R. Castañeda, A. Kannt, C. M. P. Rodrigues, S. Cockell, O. Govaere, A. K. Daly, M. Allison, K. Honnens de Lichtenberg, Y. O. Kim, A. Lindblom, S. Oldham, A.-C. Andréasson, F. Schlerman, J. Marioneaux, A. Sanyal, M. B. Afonso, R. Younes, Y. Amano, S. L. Friedman, S. Wang, D. Bhattacharya, E. Simon, V. Paradis, A. Burt, I. M. Grypari, S. Davies, A. Driessen, H. Yashiro, S. Pors, M. Worm Andersen, M. Feigh, C. Yunis, P. Bedossa, M. Stewart, H. L. Cater, S. Wells, J. M. Schattenberg, Q. M. Anstee, D. Tiniakos, J. W. Perfield, E. Petsalaki, P. Davidsen and A. Vidal-Puig, An unbiased ranking of murine dietary models based on their proximity to human metabolic dysfunction-associated steatotic liver disease (MASLD), *Nat. Metab.*, 2024, **6**, 1178–1196, DOI: 10.1038/s42255-024-01043-6.

37 D. Sun, J. Zhu, G. Zeng, X. Yang, X. Zhu, D. Aierken, Z. Shi, S. Ding, J. Ge, H. Hu and X. Yang, HDC/histamine signaling axis drives macrophage reprogramming to promote angiogenesis in hindlimb-ischemic mice, *Int. J. Biol. Sci.*, 2025, **21**, 2508–2530, DOI: 10.7150/ijbs.105148.

38 A. K. Ghosh, N. Hirasawa, H. Ohtsu, T. Watanabe and K. Ohuchi, Defective angiogenesis in the inflammatory granulation tissue in histidine decarboxylase-deficient mice but not in mast cell-deficient mice, *J. Exp. Med.*, 2002, **195**, 973–982, DOI: 10.1084/jem.20011782.

39 V. V. Raveendran, X. Tan, M. E. Sweeney, B. Levant, J. Slusser, D. J. Stechschulte and K. N. Dileepan, Lipopolysaccharide induces H1 receptor expression and enhances histamine responsiveness in human coronary artery endothelial cells, *Immunology*, 2011, **132**, 578–588, DOI: 10.1111/j.1365-2567.2010.03403.x.

40 F. Cianchi, C. Cortesini, N. Schiavone, F. Perna, L. Magnelli, E. Fanti, D. Bani, L. Messerini, V. Fabbroni, G. Perigli, S. Capaccioli and E. Masini, The role of cyclooxygenase-2 in mediating the effects of histamine on cell proliferation and vascular endothelial growth factor production in colorectal cancer, *Clin. Cancer Res.: Off. J. Am. Assoc. Cancer Res*, 2005, **11**, 6807–6815, DOI: 10.1158/1078-0432.CCR-05-0675.

41 J. Shen, Z. Tong, B. Han, Z. Zhang, Z. Xian, Y. Yuan, X. Duan, S. Han, P. Liu and Z. Wang, Synergistic wound healing: unraveling the multi-target effects of traditional chinese medicine and its biomaterials on chronic wound pathways, *Int. J. Nanomed.*, 2025, **20**, 12889–12912, DOI: 10.2147/IJN.S513585.

42 Zulfareen, A. Taiyab, G. M. Hasan and M. I. Hassan, A review on the role of pyruvate kinase M2 in cancer: from metabolic switch to transcriptional regulation, *Int. J. Biol. Macromol.*, 2025, **330**, 148067, DOI: 10.1016/j.ijbiomac.2025.148067.

43 S. Smolinska, E. Winiarska, A. Globinska and M. Jutel, Histamine: a mediator of intestinal disorders-a review, *Metabolites*, 2022, **12**, 895, DOI: 10.3390/metabo12100895.

44 X. Liu, X. Lu, H. Nie, J. Yan, Z. Ma, H. Li, S. Tang, Q. Yin and J. Qiu, *Lactobacillus* from fermented bamboo shoots prevents inflammation in DSS-induced colitis mice *via* modulating gut microbiome and serum metabolites, *Food Sci. Hum. Wellness*, 2024, **13**, 2833–2846, DOI: 10.26599/FSHW.2022.9250229.

45 J. Zhang, Z. Sun, L. Cheng, J. Kang, Y. Liu, Y. Zhao, M. Xiao, H. Liu, Q. Zhu, Q. Guo and C. Lin, Structural characterization of water-soluble pectin from the fruit of diospyros lotus L. and its protective effects against DSS-induced colitis in mice, *J. Agric. Food Chem.*, 2025, **73**, 1630–1641, DOI: 10.1021/acs.jafc.4c07611.

46 W. Gu, L. Zhang, T. Han, H. Huang and J. Chen, Dynamic changes in gut microbiome of ulcerative colitis: initial study from animal model, *J. Inflamm. Res.*, 2022, **15**, 2631–2647, DOI: 10.2147/JIR.S358807.

47 K. Nishino, A. Nishida, R. Inoue, Y. Kawada, M. Ohno, S. Sakai, O. Inatomi, S. Bamba, M. Sugimoto, M. Kawahara, Y. Naito and A. Andoh, Analysis of endoscopic brush samples identified mucosa-associated dysbiosis in inflammatory bowel disease, *J. Gastroenterol.*, 2018, **53**, 95–106, DOI: 10.1007/s00535-017-1384-4.

48 C. Lee, S. N. Hong, N. Y. Paik, T. J. Kim, E. R. Kim, D. K. Chang and Y.-H. Kim, CD1d modulates colonic inflammation in NOD2−/− mice by altering the intestinal microbial composition comprising acetatifactor muris, *J. Crohns Colitis*, 2019, **13**, 1081–1091, DOI: 10.1093/ecco-jcc/jjz025.

49 X. Liu, B. Mao, J. Gu, J. Wu, S. Cui, G. Wang, J. Zhao, H. Zhang and W. Chen, Blautia—a new functional genus with potential probiotic properties?, *Gut Microbes*, 2021, **13**, 1875796, DOI: 10.1080/19490976.2021.1875796.

50 Y. Zhang, Y. Wang, X. Zhang, P. Wang, F. Shi, Z. Zhang, R. Wang, D. Wu and J. She, Gastrointestinal self-adaptive and nutrient self-sufficient akkermansia muciniphila-gelatin porous microgels for synergistic therapy of ulcerative colitis, *ACS Nano*, 2024, **18**, 26807–26827, DOI: 10.1021/acsnano.4c07658.

51 H. Zhang, Y. Pan, Y. Jiang, M. Chen, X. Ma, X. Yu, D. Ren and B. Jiang, Akkermansia muciniphila ONE effectively ameliorates dextran sulfate sodium (DSS)-induced ulcerative colitis in mice, *NPJ Sci. Food*, 2024, **8**, 97, DOI: 10.1038/s41538-024-00339-x.

52 J. Wang, H. Gu, H. Gao, T. Zhang, F. Jiang, P. Song, Y. Liu, Q. Fan, Y. Xu and R. Zhang, Insights into cold-season adaptation of mongolian wild asses revealed by gut microbiome metagenomics, *Microorganisms*, 2025, **13**, 2304, DOI: 10.3390/microorganisms13102304.

53 J. Niño-Narvión, M. I. Rojo-López, P. Martinez-Santos, J. Rossell, A. J. Ruiz-Alcaraz, N. Alonso, B. Ramos-Molina, D. Mauricio and J. Julve, NAD^+ precursors and intestinal inflammation: therapeutic insights involving gut microbiota, *Nutrients*, 2023, **15**, 2992, DOI: 10.3390/nu15132992.

54 Z. Wang, N. Iida, J. Seishima, H. Okafuji, M. Yutani, Y. Fujinaga, Y. Hashimoto, H. Tomita, E. Mizukoshi and S. Kaneko, Patient-derived enterococcus faecium with inflammatory genotypes promote colitis, *J. Gastroenterol.*, 2022, **57**, 770–783, DOI: 10.1007/s00535-022-01905-4.

55 Y. Lin, X. Zhou, S. Xie, J.-A. Huang, J. Li, Y. Yao, M. Li, J. Bo, L. Xiao, Z. Liu and W. Quan, Unlocking the healing power of jinhua white tea fermented by eurotium cristatum using the unique ''flowering'' technology: a promising ally against inflammatory bowel disease, *Food Res. Int.*, 2025, **213**, 116555, DOI: 10.1016/j.foodres.2025.116555.